Mon. Not. R. Astron. Soc. **272**, 544–550 (1995)

Neutral hydrogen at high redshifts as a probe of structure formation – II. Line profile of a protocluster

A. Kumar,[1] T. Padmanabhan[2] and K. Subramanian[1]

[1] *National Centre for Radio Astrophysics, Tata Institute of Fundamental Research, Pune University Campus, Ganeshkind, Pune 411007, India*
[2] *Inter University Centre for Astronomy and Astrophysics, Pune University Campus, Ganeshkind, Pune 411007, India*

Accepted 1994 September 5. Received 1994 June 20

ABSTRACT

The formation of structures at $z \lesssim 10.0$ can be probed using the 21-cm line emission from the neutral hydrogen. Two of us (KS and TP, Paper I) previously computed the expected abundance of protoclusters as a function of the flux density at various redshifts, in the cold dark matter (CDM) and the hot dark matter (HDM) models. As a complement to Paper I, here we work out in detail how the H I line profile from a spherically symmetric protocluster evolves as it decouples from Hubble expansion and collapses. Our paradigm for structure formation is the CDM model where structures form hierarchically. Neutral hydrogen, in the small-scale clumps that form the protocluster, is the source of H I line emission. We find that the peak fluxes of the H I line profile in this model are typically of order 0.5–0.7 mJy, while the widths (FWHM) are of order 0.3–1.8 MHz. The major uncertainty in our calculations is the fraction of mass of the protocluster in the form of neutral hydrogen. If the neutral hydrogen fraction f is of the order of the value we have adopted ($f = 0.025$) in our calculations or greater, then a typical protocluster could indeed be detectable by future facilities, like the Giant Metrewave Radio Telescope (GMRT) which is currently being built in India. If the neutral hydrogen fraction is much less than the value we have adopted, then a more sensitive instrument is needed to detect the H I line emission from a typical protocluster.

Key words: galaxies: formation – dark matter – large-scale structure of Universe – radio lines: general.

1 INTRODUCTION

Galaxies and large-scale structures in the Universe are thought to have originated by the growth of small initial density perturbations via gravitational instability. In this scenario, it should be possible to detect any neutral hydrogen that might have existed in the protocondensates by observing the redshifted 21-cm line emission (Sunyaev & Zeldovich 1972, 1974). Detection of such a protocluster will put severe constraints on the theories of structure formation.

Several searches for the redshifted 21-cm line have so far yielded only null results (cf. Subrahmanyan & Anantharamaiah 1990; Subrahmanyan & Swarup 1990; Uson, Bagri & Cornwell 1991a; Wieringa, de Bruyn & Katgert 1992, and references therein). A positive detection of redshifted 21-cm emission was reported by Uson, Bagri & Cornwell (1991b), but it has not been confirmed by subsequent observations (Briggs, Sorar & Taramopoulos 1993; de Bruyn & Katgert 1994, in preparation). Future facilities like the GMRT, presently being constructed in India (Swarup 1984), are expected to act as sensitive instruments for detecting such protocondensates. It is therefore interesting to work out the abundances of such protocondensates, expected fluxes and other properties of the redshifted 21-cm line, in various models of structure formation, and to compare the results with the expected sensitivity limits of future instruments.

Note that definitive predictions about the 21-cm emission from a protocondensate, in different theories of structure formation, could not be made in the past, because of the uncertainty in the amplitude of the power spectrum; however, the detection of the temperature anisotropies of the cosmic microwave background radiation (CMBR) by the *COBE* satellite (Smoot et al. 1992) has improved the situation. Using *COBE* results, one can unambiguously fix the amplitude of the power spectrum in any model, and thus make reliable calculations and compare the different models with the observations.

In an earlier paper (Subramanian & Padmanabhan 1993,

Paper I hereafter), two of us computed the expected abundance of protocondensates that will emit a flux higher than S, at various redshifts, in the CDM and HDM models, normalized to the *COBE* data. One important result of these calculations is that cluster-size objects as predicted by the HDM models are unlikely to have formed at $z>2$ and therefore cannot be the source of 21-cm emission at high redshift. In a hierarchical model of structure formation like CDM model, however, collapse occurs on subgalactic scales first and progressively on larger scales later. If the gas can cool efficiently, these small-scale clumps may become the source of H I emission. In fact, there is observational evidence to indicate that neutral hydrogen exists in the Universe in the form of clumps, although the absence of a Gunn–Peterson dip in the ultraviolet spectra of quasars rules out the presence of any smoothly distributed neutral hydrogen in the Universe at $z \leq 4$–5 (Gunn & Peterson 1965; Jenkins & Ostriker 1991; Giallongo et al. 1994). In particular, the damped Lyα systems may contain as much mass in the neutral hydrogen as is present in the total stellar content of all present-day disc galaxies (Wolfe et al. 1986; Turnshek et al. 1989; Wolfe 1989; Lanzetta et al. 1991). In such a case, it may be possible to detect the protoclusters even at redshifts as high as $z \sim 5$.

Here, we complement the study in Paper I by working out in detail how the H I line profile from a single protocluster evolves as it decouples from Hubble expansion and collapses. Our calculations assume that (i) the protocluster consists of small-scale clumps of H I gas, as is likely in hierarchical clustering theories of galaxy formation (Subramanian & Swarup 1992; Paper I) and (ii) the density profile of the protoclusters is spherically symmetric and the density contrast is a non-increasing function of the radius. In Paper I, we assumed a spherical top hat density profile. Here we relax this condition and test the sensitivity of the results to changes in the assumed density profile.

This paper is organized as follows. In the next section, we set up the mathematical formulation to compute the evolution of the line profile of a protocluster, given its initial density distribution. Detailed numerical results of our computations are given in Section 3, where we also discuss the detectability of a protocondensate. Section 4 gives a short summary of the results.

2 EVOLUTION OF THE LINE PROFILE

Consider a spherically symmetric perturbation with excess density contrast $\delta_i(r_i)$ at an early epoch t_i. For the sake of convenience, let us assume that $\delta_i(r_i)=0$ for $r_i > R_i$, where R_i is the proper radius of the protocluster at t_i. As the protocluster evolves, shells at larger and larger radii decouple from the Hubble expansion, turn around and collapse. If we assume that $\delta_i(r_i)$ is a non-increasing function of r_i, it follows that shells of different radii never cross each other. In such a case, the mass contained inside any given shell is a constant, making the force F on a shell inversely proportional to the square of the radius r of the shell at that epoch. Therefore we can easily integrate the equation of motion to get $r(r_i, t)$, where r is the radius of the shell at time t, whose initial radius at time t_i is r_i, in the parametric form

$$r(t)=\frac{r_i}{2\overline{\delta}_i(r_i)}(1-\cos\psi), \tag{1}$$

$$t=\frac{3}{4}\frac{t_i}{\overline{\delta}_i(r_i)^{3/2}}(\psi-\sin\psi). \tag{2}$$

Here, ψ is an evolution angle, which characterizes how far each shell has progressed towards collapse. One can also derive how density $\rho(r, t)$ evolves with time using mass conservation (Peebles 1980; Padmanabhan & Subramanian 1992). In a $\Omega=1$ universe, one gets

$$\frac{\rho(r,t)}{\rho_b(t)}= \frac{[9(\psi-\sin\psi)^2/2(1-\cos\psi)^3]}{1-3[(\delta_i/\overline{\delta}_i)-1]\{1-[3\sin\psi(\psi-\sin\psi)/2(1-\cos\psi)^2]\}}, \tag{3}$$

where $\rho_b(t)$ is the background density of the universe and $\overline{\delta}_i(r_i)$ is the average excess density contrast within the sphere of radius r_i at time t_i.

It is convenient to express the above relations in terms of the comoving radius $x=[a(t_0)/a(t_i)]r_i=(1+z_i)r_i$ and the average excess density contrast inside the shell at the present epoch, assuming linear growth, $\overline{\delta}_0(x)=\langle\delta_0(x)\rangle=(3/5)(1+z_i)\overline{\delta}_i(r_i)$, instead of r_i and $\overline{\delta}_i(r_i)$, respectively. In terms of x and $\overline{\delta}_0(x)$, and using $a(t)\propto t^{2/3}$, we get

$$r(x,\psi)=\frac{3x}{10\overline{\delta}_0(x)}(1-\cos\psi), \tag{4}$$

$$t(x,\psi)=\left(\frac{3}{5}\right)^{3/2}\frac{3}{4}\frac{t_0}{\overline{\delta}_0(x)^{3/2}}(\psi-\sin\psi), \tag{5}$$

where t_0 is the age of the universe at the present epoch. The radial velocity $v(x, \psi)=(dr/dt)=(dr/d\psi)(d\psi/dt)$ of each shell can be calculated from (4) and (5):

$$v(x,\psi)=\frac{2}{5}\left(\frac{5}{3}\right)^{3/2}\overline{\delta}_0(x)^{1/2}\frac{x}{t_0}\frac{\sin\psi}{(1-\cos\psi)}. \tag{6}$$

If we use redshift z as the time coordinate, then (5) can be written as

$$(1+z)=\frac{5}{3}\left(\frac{4}{3}\right)^{2/3}\overline{\delta}_0(x)(\psi-\sin\psi)^{-2/3}. \tag{7}$$

For any shell of comoving radius x, equation (7) determines the evolution angle ψ at redshift z. For example, the turn around redshift z_{coll} of a shell of comoving radius x is given by putting $\psi=\pi$ (because $v=0$ at $\psi=\pi$), i.e.

$$(1+z_{coll})=\frac{5}{3}\left(\frac{4}{3\pi}\right)^{2/3}\overline{\delta}_0(x). \tag{8}$$

From (8), we see that shells of larger and larger radii turn around at later epochs in any model with a decreasing $\overline{\delta}_0(x)$. On the other hand, for a spherical top hat model, $\overline{\delta}_0(x)$ is a constant, and hence all the shells turn around at the same epoch,

$$(1+z_{coll})=\frac{5}{3}\left(\frac{4}{3\pi}\right)^{2/3}\overline{\delta}_0(0)=\frac{\overline{\delta}_0(0)}{1.686}. \tag{9}$$

In our calculations, we consider the optical depth of the protocluster to be sufficiently small. Hence the energy

radiated by the protocondensate is given by adding the energies of the individual photons emitted by each hydrogen atom. However, at any given phase in the evolution of the protocluster, different volume elements will each have a different line-of-sight velocity, v_Z, which depends on the comoving radius of the element x (see equation 6) and on the angle θ made by the radius vector from the centre of the protocluster to the volume element with the line of sight. Hence the 21-cm radiation will be redshifted differently for different elements. This effect should be properly taken into account in calculating the emissivity (energy emitted per unit time per unit frequency) by adding over the individual volume elements.

Let us consider a protocluster at redshift z. In the following equations, we suppress the dependence on physical quantities ρ, v_Z, etc. on redshift z, as it is just a parameter in all the equations. In general, some of the outer shells will be expanding, shells nearer the core will be collapsing and one shell will be at the point of turn-around. This situation is illustrated in Fig. 1. The energy emitted per unit time in 21-cm line radiation from a small volume element $\mathrm{d}X\,\mathrm{d}Y\,\mathrm{d}Z$ of the protocluster is

$$\mathrm{d}E = \frac{3}{4} A_{21} h \nu_e \frac{\rho_{\mathrm{H\,I}}(X, Y, Z)}{m_p} \mathrm{d}X\,\mathrm{d}Y\,\mathrm{d}Z. \tag{10}$$

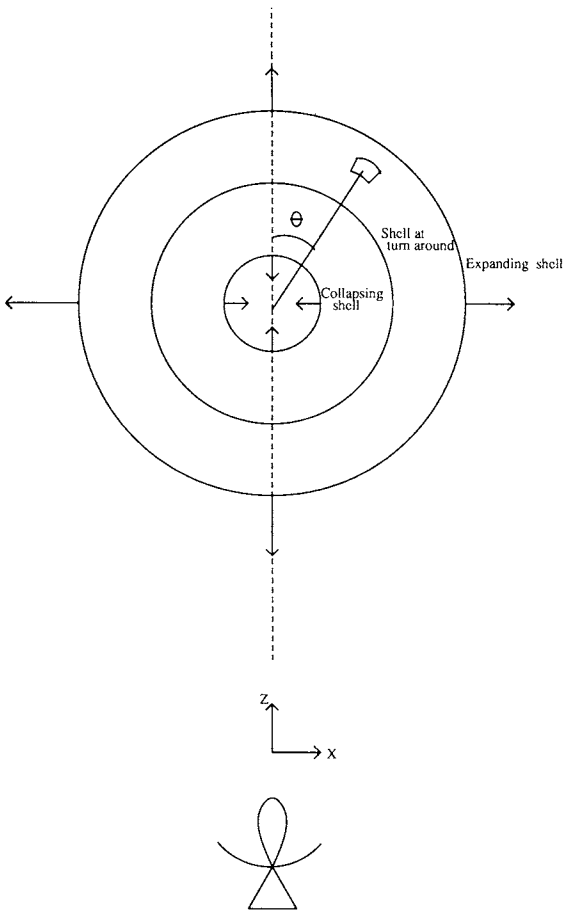

Figure 1. A snapshot of a typical protocluster in one of its phases of evolution. The dotted line is the direction of the line of sight. The angle θ is the angle made by the radius vector to a volume element at (r, θ, ϕ) with the line of sight.

Here, A_{21} is the spontaneous emission rate, ν_e is the frequency of the 21-cm photon (1420.4 MHz), m_p is the proton mass and $\rho_{\mathrm{H\,I}}$ is the neutral hydrogen density, which we take to be a fraction, f say, of the total mass density. If we choose the Z-axis along the line of sight (see Fig. 1), then the observed frequency ν is related to v_Z as

$$\nu = \nu_e \left[1 - \frac{v_Z(X, Y, Z)}{c}\right], \tag{11}$$

$$\frac{\partial \nu}{\partial Z} = -\frac{\nu_e}{c} \frac{\partial v_Z}{\partial Z} \tag{12}$$

Inverting (11), we can express the Z-coordinate in terms of X, Y and ν: $Z = Z(X, Y, \nu)$. Therefore we have

$$\mathrm{d}E = -\frac{3}{4} A_{21} h c \frac{\rho_{\mathrm{H\,I}}[X, Y, Z(X, Y, \nu)]}{m_p} \frac{1}{\partial v_Z[X, Y, Z(X, Y, \nu)]/\partial Z} \mathrm{d}X\,\mathrm{d}Y\,\mathrm{d}\nu \tag{13}$$

The quantity $\mathrm{d}E(X, Y, \nu)/\mathrm{d}\nu$ gives the brightness distribution in the plane of the sky as a function of frequency. Integrating over the sky plane, we get the emissivity $(\mathrm{d}u/\mathrm{d}\nu)$ of the protocluster. Dividing this by $4\pi D_L^2$, where D_L is the luminosity distance, we get the line profile (flux versus frequency) of the protocluster.

In general, for an asymmetric collapse, it is difficult to invert (11) to get $Z = Z(X, Y, \nu)$. In the spherically symmetric case, however, it is easy to calculate the emissivity of the protocondensate, if we use spherical coordinates (r, θ, ϕ). Here, θ is the angle made by the radius vector to the volume element $\mathrm{d}V$ with the line of sight (see Fig. 1). The frequency of the radiation from the volume element $\mathrm{d}V$ located at (r, θ, ϕ) is

$$\nu = \nu_e \left[1 - \frac{v(r)}{c} \cos\theta\right] \tag{14}$$

so that

$$\frac{\partial \nu}{\partial \theta} = \frac{\nu_e}{c} v(r) \sin\theta. \tag{15}$$

Note that the frequency ν does not depend on the azimuth ϕ. Energy emitted by the volume element $r^2\,\mathrm{d}r \sin\theta\,\mathrm{d}\theta\,\mathrm{d}\phi$ is given by

$$\mathrm{d}E = \frac{3}{4} A_{21} h \nu_e \frac{\rho_{\mathrm{H\,I}}(r)}{m_p} r^2\,\mathrm{d}r \sin\theta\,\mathrm{d}\theta\,\mathrm{d}\phi. \tag{16}$$

Now, using (15), (16) can be written as

$$\mathrm{d}E = \frac{3}{4} A_{21} \frac{hc}{m_p} \frac{\rho_{\mathrm{H\,I}}(r) r^2}{v(r)} \mathrm{d}r\,\mathrm{d}\phi\,\mathrm{d}\nu. \tag{17}$$

Integrating the above equation over (r, ϕ), we get the emissivity $\mathrm{d}u_{\mathrm{rad}}/\mathrm{d}\nu$ (the subscript 'rad' is used to denote that this emissivity is due to the radial motion of the protocluster. This has to be convolved with a Gaussian to take into account the internal velocity dispersion of the small-scale

clumps; see below). Therefore

$$\frac{du_{\rm rad}}{d\nu}(\nu)=\int_0^R g(r)\,dr, \tag{18}$$

where R is the proper radius of the protocondensate at redshift z. Here,

$$g(r)=(3\pi/2)A_{21}(hc/m_{\rm p})[\rho_{\rm H_I}(r)r^2/v(r)], \tag{19}$$

if $\cos(\theta)=[c/v(r)][1-(\nu/\nu_{\rm e})]$ has a real solution and is zero otherwise.

The expression for emissivity in (18) gives the emissivity due to the radial expansion and collapse of the protocluster. However, the small-scale structures themselves have internal velocity dispersion $\sigma_v=100$–200 km s^{-1}. We can take this into account by convolving $(du_{\rm rad}/d\nu)$ with a normalized Gaussian $h(\nu)$ of width $\sigma_v=100$–200 km s^{-1} [in terms of frequency units, the corresponding λ rms deviation is $\sigma_{\rm w}=0.473$–0.947 MHz]. Therefore the actual emissivity $du/d\nu$ of the protocluster is given by

$$\frac{du}{d\nu}(\nu)=A\int_{-\infty}^{+\infty}\frac{du_{\rm rad}}{d\nu'}\exp[-(\nu-\nu')^2/2\sigma_{\rm w}^2]\,d\nu' \tag{20}$$

where $h(\nu)=A\exp(-\nu^2/2\sigma_{\rm w}^2)$ and $A=1/(\sigma_{\rm w}\sqrt{2\pi})$.

To compute the observed flux $F(\nu_0)$, we divide the emissivity by $4\pi D_{\rm L}^2$ and obtain

$$F(\nu_0)=\frac{1}{4\pi D_{\rm L}^2}\frac{du}{d\nu}(\nu), \tag{21}$$

where $\nu_0=\nu(1+z)^{-1}$ and $D_{\rm L}=2cH_0^{-1}[(1+z)-(1+z)^{1/2}]$ in an $\Omega=1$ universe. In our calculations, we have chosen $H_0=50\,h_{50}$ km s^{-1} Mpc^{-1}.

We shall now discuss the results of the computation.

3 RESULTS

For explicit computations we have adopted an initial density profile of the form

$$\begin{aligned}\delta_0(x)&=\delta_0(0)[1+(x/a)^2]^{-\alpha} && (\text{for } x\le R),\\ &=0 && (\text{for } x>R).\end{aligned} \tag{22}$$

We have calculated the line profile for $\alpha=0$, 1, 3/2 and 5/2. For $\alpha=0$, we have the spherical top hat model in which the excess density contrast is a constant within the protocluster. As mentioned earlier, we used this density profile in Paper I for calculating the abundances of the protocluster in CDM and HDM models. Models with $\alpha=1$ describe an isothermal sphere, with $\alpha=3/2$ correspond to the King's model, and with $\alpha=5/2$ describe a more centrally concentrated density model. For a given initial density profile, there are three independent free parameters: comoving radius R, scalelength a and central density contrast $\delta_0(0)$. We fix R by demanding that the mass of the protocluster is $m\times10^{15}$ M$_\odot$, where $m=1$ or 2. We choose $a=3$ Mpc for $m=1$, and $a=4$ Mpc for $m=2$. In the CDM model, $\overline{\delta}_0$ is a Gaussian random variable with zero mean and a variance of $\sigma(R)$. We fix $\delta_0(0)$ by imposing the condition that $\overline{\delta}_0(R)=n\times\sigma_{\rm CDM}(R)$, where $\sigma_{\rm CDM}(R)$ is the mean square fluctuation of the mass in a sphere of radius R in the CDM model, normalized to *COBE* results (cf. Padmanabhan & Narasimha 1992; Paper I). We choose n to be in the range 1–3 (note that this is the only model we consider here). The probability of finding a protocluster with excess density contrast $3\sigma_{\rm CDM}$ is about $e^{-4.5}=0.01$ times smaller than that of finding a more typical protocondensate with excess density contrast $1\sigma_{\rm CDM}$. The major uncertainty in our calculations is the neutral hydrogen content in the form of smaller scale clumps. Let $f_{\rm coll}$ be the mass fraction of the protocluster in the form of clumps. Of this, we will assume a fraction $f_{\rm b}$ to be in the form of baryons. If a fraction $f_{\rm N}$ of the baryons is in the neutral hydrogen form, then the density $\rho_{\rm H_I}$ of neutral hydrogen in the clumped form in the protocluster is given by

$$\rho_{\rm H_I}=f_{\rm N}f_{\rm b}f_{\rm coll}\rho\equiv f\rho,$$

where $f=f_{\rm N}f_{\rm b}f_{\rm coll}$. For a set of values $f_{\rm coll}\approx0.5$, $f_{\rm b}\approx0.1$ and $f_{\rm N}\approx0.5$, we have $f\sim0.025$. To fix ideas, we have therefore taken the neutral hydrogen fraction in the form of clumps to be $f=0.025$ (see also Paper I and Subramanian & Swarup 1992).

As the shells turn around and collapse, the density in the core of the protocluster increases arbitrarily, resulting in the large increase of flux from the protocluster (see equation 18). In reality, this will not happen, since, as the protocluster collapses, it is likely to virialize and heat up the gas, destroying the neutral hydrogen long before this epoch. So, we have to cut off the contributions to the flux from the shells that have collapsed to a radius less than a critical value $r_{\rm c}$. Here, we have taken this critical value $r_{\rm c}$ of any shell to be half its turn-around radius.

We now discuss the results of this analysis. In Fig. 2, we plot the emitted luminosity per unit velocity range v_Z (in units of 10^{25} erg s^{-1} Hz^{-1}) at different stages of the evolution ($z=8.5$, 5.1 and 3.34) of the protocluster, modelled to be a $1\sigma_{\rm CDM}$ fluctuation with $\alpha=1$. Since the energy emitted by a shell is inversely proportional to the radial velocity $v(r)$ (see equation 16), it can be arbitrarily high from the shell near turn-around. To make the program numerically stable, we have cut off the contributions to the emissivity from the shells that have radial velocity $v\le10$ km s^{-1}. The emissivity

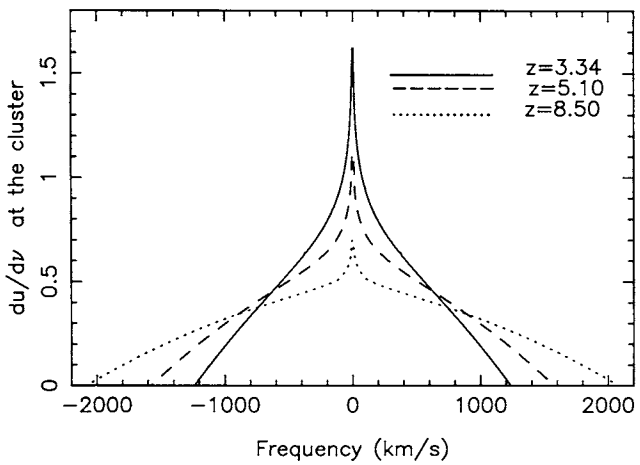

Figure 2. The emissivity line profile at different stages of the evolution ($z=8.5$, 5.1 and 3.34) of the protocondensate for $\alpha=1$, taking the protocondensate to be a $1\sigma_{\rm CDM}$ fluctuation.

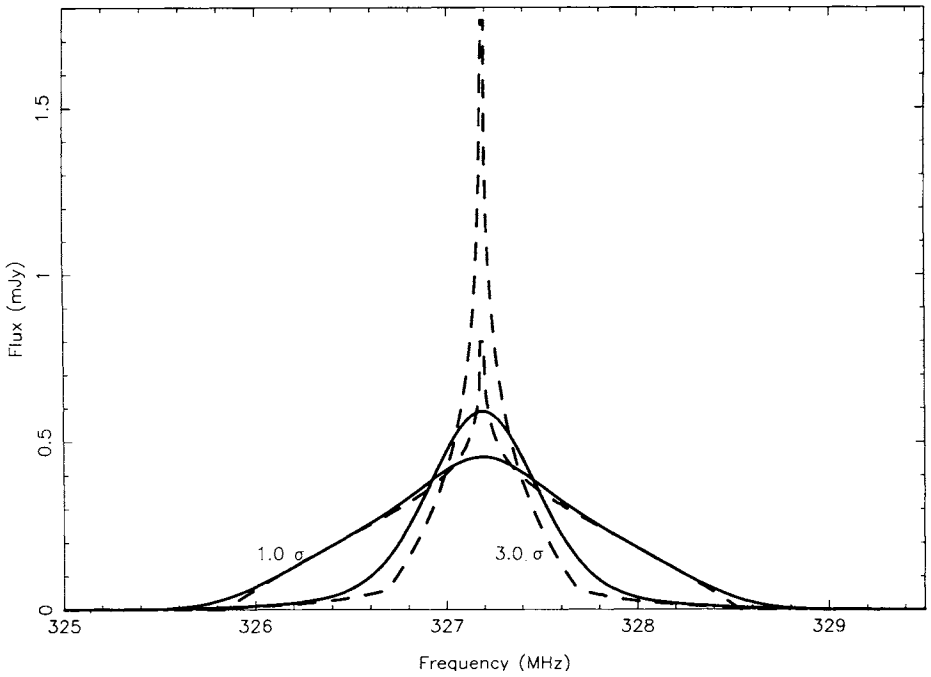

Figure 3. The raw and the convolved ($\sigma_v = 200$ km s^{-1}) line profiles (flux versus frequency) for $z = 3.34$, for both a $1\sigma_{\rm CDM}$ and a $3\sigma_{\rm CDM}$ fluctuation. Solid and dashed lines correspond to the convolved and raw profiles, respectively.

profile consists of two components, one narrow core component due to shells near turn-around and a broad hump of width 600–800 km s^{-1} arising from the expanding and collapsing shells with a large peculiar velocity. It can be seen that, as the shells of larger and larger radii turn around at later epochs (i.e. at smaller z), the peak of the core component increases while its width decreases.

Some sample line profiles (flux versus frequency), resulting from the collapse of a protocluster with $M = 10^{15}$ M$_\odot$, are shown in Fig. 3 for $z = 3.34$, one of the redshifts probed by GMRT. We have adopted a value of $\alpha = 1$ to compute the line profile, and considered two different values of the initial density contrast, $\overline{\delta}_0(R) = \sigma_{\rm CDM}$ and $\overline{\delta}_0(R) = 3\sigma_{\rm CDM}$. Note that, as mentioned earlier, the line profile due to the radial motion of the shells has to be convolved with a normalized Gaussian to take into account the internal velocity dispersion. This will give a peak of finite height $v_Z = 0$, irrespective to the cut-off of $v \leq 10$ km s^{-1} of subclumps making up the protocluster. In Fig. 3, we have convolved the raw line profile by a Gaussian of width $\sigma_v = 200$ km s^{-1}. Solid and dashed lines correspond to the convolved and raw profiles, respectively. The peak fluxes of the convolved line profiles, for $\overline{\delta}_0(R) = \sigma_{\rm CDM}$ and $\overline{\delta}_0(R) = 3\sigma_{\rm CDM}$ are 0.46 and 0.59 mJy, while the linewidths (FWHM) are 1.355 and 0.694 MHz, respectively.

We have also computed the line profiles, at $z = 3.34$, for various other values of the parameters of the protocluster. The results of these computations are summarized in Tables 1 and 2. There, we have given the peak fluxes ($F_{\rm peak}$) and linewidths $\Delta\nu$ (FWHM) for various initial density contrasts of the protocluster and different values of σ_v. We have adopted an initial density profile with $\alpha = 1$. Table 1 gives the results for a mass $M = 10^{15}$ M$_\odot$, while in Table 2 we have taken a larger $M = 2 \times 10^{15}$ M$_\odot$. For a protocluster of mass $M = 10^{15}$ M$_\odot$, the peak flux ranges from ~0.5–1.1 mJy, while the linewidths range over 0.3–1.4 MHz, the smaller width corresponding to the larger flux. For a larger mass the peak flux increases by a factor ~1.5–1.8, and the linewidth increases by about ~1.3–1.5. This would make the line

Table 1. Peak fluxes, linewidths and angular size of a protocluster of mass $M = 10^{15}$ M$_\odot$, for different initial density contrasts and smoothing velocities (parametrized by n and σ_v, respectively). θ_t is the angular size of the mass, that has turned around and is collapsing.

		$\sigma_v(kms^{-1})$			
		50	100	150	200
$n \downarrow$					
1	F_{peak} (mJy)	0.60	0.53	0.49	0.46
	$\Delta\nu$ (MHz)	0.900	1.117	1.251	1.355
	θ_t $(arc\ min)$	1.88			
2	F_{peak} (mJy)	0.90	0.74	0.65	0.58
	$\Delta\nu$ (MHz)	0.430	0.635	0.776	0.903
	θ_t $(arc\ min)$	3.12			
3	F_{peak} (mJy)	1.08	0.84	0.69	0.59
	$\Delta\nu$ (MHz)	0.298	0.447	0.572	0.687
	θ_t $(arc\ min)$	4.02			

Table 2. Peak fluxes, linewidths and angular size of a protocluster of mass $M=2\times10^{15}$ $M_\odot$, for different initial density contrasts and smoothing velocities (parametrized by n and σ_v, respectively). θ_t is the angular size of the mass that has turned around and is collapsing.

		$\sigma_v(kms^{-1})$			
		50	100	150	200
$n\downarrow$					
1	F_{peak} (mJy)	0.88	0.79	0.74	0.70
	$\Delta\nu$ (MHz)	1.346	1.589	1.735	1.846
	θ_t $(arc\ min)$	1.88			
2	F_{peak} (mJy)	1.33	1.13	1.01	0.93
	$\Delta\nu$ (MHz)	0.600	0.832	1.022	1.159
	θ_t $(arc\ min)$	3.33			
3	F_{peak} (mJy)	1.67	1.37	1.20	1.08
	$\Delta\nu$ (MHz)	0.410	0.599	0.753	0.892
	θ_t $(arc\ min)$	4.40			

easier to detect by a factor of ~ 1.5 (see below). As expected, the peak flux decreases with an increase in σ_v while the linewidth increases. It is also the case that the peak flux increases and the linewidth decreases for protoclusters with larger initial density contrast. This arises because a larger σ fluctuation has more matter near turn-around at the redshift we have considered.

Let us consider the detectability of a typical protocondensate with an instrument like the GMRT. The instrumental parameters of the GMRT are given by Swarup et al. (1991) and have been discussed in Paper I, in this context. The expected σ_{rms} due to the thermal noise in GMRT at the frequency 327 MHz, for a 10-h integration and a bandwidth of 300 KHz, is about 0.16 mJy, taking into account only the antennas in the central array. This estimate is relevant for a source smaller than the synthesized beam of the telescope, which is about 3.2 arcmin. Note that, to get the best signal-to-noise ratio, the angular resolution of the telescope should be comparable to the source size.

In Tables 1 and 2, we have also given a characteristic angular radius θ_t, associated with the protocluster. This has been defined to be the angular radius of the shell that has just turned around. We have taken the radius of the shell that is turning around instead of the cut-off radius of the protocluster, because the contribution to the flux from the protocluster is dominated by the shells near turn-around. From Tables 1 and 2, it is clear that θ_t is smaller than the synthesized beamsize in most cases and so falls within the beam. Also, for a factor of 2 increase in the beamsize, σ_{rms} increases very little (only by a factor of about 1.3; R. Subramanyan, private communication). So, the value of σ_{rms} given above should provide a reasonable estimate for extended protoclusters as well.

We will now consider the operational criteria for the detection of a line. We may consider a line as detectable if (1) the peak of the line is above $5\sigma_{rms}$, and (2) there are at least a few observed points, say 3 to 5, above $2\text{–}4\sigma_{rms}$. These criteria, however, can be applied only after we have fixed the frequency resolution, $\Delta\nu_s$, that we are using, since $\sigma_{rms}\propto(\Delta\nu_s)^{-1/2}$. We take the value of $\Delta\nu_s$ to be in the range $(0.25\text{–}0.5)\Delta\nu$, so that 3–5 points on the line have fluxes greater than or equal to $F_{peak}/2$.

Let us consider a typical example of a protocluster with mass $M=10^{15}$ $M_\odot$, modelled as a $2\sigma_{CDM}$ fluctuation, with $\alpha=1$ and $\sigma_v=150$ km s^{-1}. From Table 1, the peak flux and the linewidth of the H I line profile of such a protocluster are $F_{peak}=0.65$ mJy and $\Delta\nu=0.776$ MHz, respectively. For a bandwidth $\Delta\nu_s=0.776/4=0.194$ MHz, we have $\sigma_{rms}=0.195$ mJy. The peak value F_{peak} is then $3.3\sigma_{rms}$. If we choose $\Delta\nu_s=0.776/2=0.388$ MHz, so that there are three points on the line that have fluxes more than $F_{peak}/2$, then the peak value is $4.7\sigma_{rms}$. Such a line will be on the threshold of detectability, according to our criteria. On the other hand, for a protocluster of mass $M=2\times10^{15}$ $M_\odot$, the peak value F_{peak}, for the case of detecting five points above $F_{peak}/2.0$, is $5.9\sigma_{rms}$, and, for a coarser resolution of $\Delta\nu/2$, F_{peak} is $8.4\sigma_{rms}$. Hence such a protocluster can indeed be detected by GMRT.

Finally, in Fig. 4 we illustrate the effect of assuming different density profiles, $\alpha=0$, 1/2, 3/2 and 5/2, for a protocluster which is a $3\sigma_{CDM}$ fluctuation. The mass of the protocluster is taken to be 10^{15} $M_\odot$. We see that a change in α from 0 to 5/2 leads to a decrease of the peak flux by a factor ≈ 2. This is basically because, in a more centrally condensed density profile (larger α), the inner shells of the protocluster turn around earlier and collapse to radii less than half the turn-around radius. This leads to a greater destruction of the H I in the innermost shells, for a larger α, and hence a decrease in flux.

4 DISCUSSIONS AND SUMMARY

In this paper, we have considered the detectability of protocondensates using redshifted 21-cm emission. For this

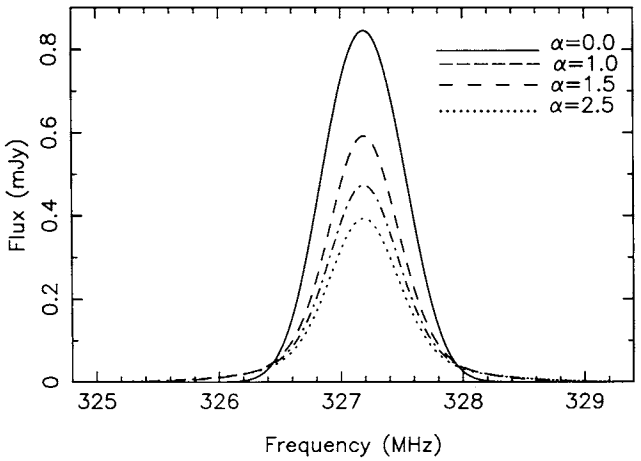

Figure 4. The convolved line profile for different initial density profiles ($\alpha=0$, 1, 3/2 and 5/2), taking the protocluster to be a $3\sigma_{CDM}$ fluctuation.

purpose, we have calculated the peak fluxes and linewidths of the H I line profile of a spherically symmetric collapsing protocluster for different initial density contrasts. Spherical symmetry allows one to write down analytic expressions for the density and the velocity fields of the protocluster. So, the sensitivity of the results to changes in the various parameters of the protocluster can be efficiently explored.

Earlier it was thought that large cluster-size pancakes, as predicted by HDM models, may be the sources of H I emission at high redshifts. However, when the initial power spectrum was normalized using *COBE* data, it was found that it is unlikely that such structures would have formed at $z \gtrsim 2$ (see Paper I). In Paper I, it was noted how the small-scale clumps could become the sources of H I emission, provided they cool efficiently. So, in this paper we have considered a large cluster-size object of mass $M \approx 10^{15}\ M_\odot$ with small-scale clumps containing neutral hydrogen, as predicted by CDM-like models, as the source of H I emission.

The calculated peak fluxes of the redshifted 21-cm line emitted by protoclusters of mass $M = 10^{15}\ M_\odot$, at $z = 3.34$, are in the range 0.5–1.1 mJy, depending on the initial density contrast and the velocity dispersion used to the smooth the line profile. The linewidths are in the range 0.3–1.4 MHz. For a typical protocluster of this mass, the peak flux is about 3–5 σ_{rms}, where σ_{rms} is the expected thermal noise in GMRT at $\nu = 327$ MHz for a 10-h integration. If the mass of the protocluster were two times larger, the peak fluxes would increase by a factor of about 1.5–1.8, and the linewidths would increase by a factor of about 1.3–1.5. In this case, the peak flux is ~ 6–$8\ \sigma_{rms}$. Such protoclusters are on the threshold of detectability by an instrument like GMRT. The major uncertainty in our calculations is the neutral fraction f, which we have taken here to be 0.025 of the total mass. The actual value of f depends on the thermal history of the gaseous component. For a different value of f, one has simply to scale the fluxes by $f/0.025$. If f is larger than the value we have adopted, it is easier to detect protoclusters, whereas if $f < 0.025$ we need a more sensitive instrument for detecting protoclusters.

ACKNOWLEDGMENTS

We thank Ravi Subrahmanyan and Govind Swarup for many useful discussions.

REFERENCES

Briggs F. H., Sorar E., Taramopoulos A., 1993, ApJ, 415, L99
Giallongo E. et al., 1994, ApJ, 425, L1
Gunn J. E., Peterson B. A., 1965, ApJ, 142, 1633
Jenkins E. B., Ostriker J. P., 1991, ApJ, 376, 33
Lanzetta K. M., Wolfe A. M., Turnshek D. A., Lu L., McMahon R. G., Hazard C., 1991, ApJS, 77, 1
Padmanabhan T., Narasimha D., 1992, MNRAS, 259, 41P
Padmanabhan T., Subramanian K., 1992, Bull. Astron. Soc. India, 20, 1
Peebles P. J. E., 1980, Large Scale Structure of the Universe. Princeton Univ. Press, Princeton, NJ
Smoot G. F. et al., 1992, ApJ, 396, L1
Subrahmanyan R., Anantharamaiah K. R., 1990, JA&A, 11, 221
Subrahmanyan R., Swarup G., 1990, JA&A, 11, 237
Subramanian K., Padmanabhan T., 1993, MNRAS, 265, 101 (Paper I)
Subramanian K., Swarup G., 1992, Nat, 359, 512
Sunyaev R. A., Zeldovich Ya. B., 1972, A&A, 20, 189
Sunyaev R. A., Zeldovich Ya. B., 1974, MNRAS, 171, 375
Swarup G., 1984, Giant Metre-Wavelength Radio Telescope – Proposal. Radio Astronomy Centre, TIFR., India
Swarup G., Ananthakrishnan S., Kapahi V. K., Rao A. P., Subrahmanya C. R., Kulkarni V. K., 1991, Current Science, 60, 95
Turnshek D. A., Wolfe A. M., Lanzetta K. M., Briggs F. H., Cohen R. D., Foltz C. B., Smith H. E., Wilkes B. J., 1989, ApJ, 344, 567
Uson J. M., Bagri D. S., Cornwell T. J., 1991a, ApJ, 377, L85
Uson J. M., Bagri D. S., Cornwell T. J., 1991b, Phys. Rev. Lett., 67, 3328
Wieringa M. H., de Bruyn A. G., Katgert P., 1992, A&A, 256, 331
Wolfe A. M., 1989, in Frenk C. S., Ellis R. S., Shanks T., Heavens A. F., Peacock J. A., eds, The Epoch of Galaxy Formation. Kluwer, Dordrecht, p. 101
Wolfe A. M., Turnshek D. A., Smith H. E., Cohen R. D., 1986, ApJS, 61, 249